ATTACHMENT IX

Review of Air Products Fischer-Tropsch Synthesis Work

During the 1980s, Air Products & Chemicals worked on several aspects of the Fischer-Tropsch synthesis. These included the development of novel Fischer-Tropsch slurry catalysts and process concepts, the design of a Fischer-Tropsch pilot plant, the hydrodynamics of bubble column reactors, and the development and operation of the LaPorte Fischer-Tropsch facility (IX.1-IX.7). Their patents concerning the preparation of Fischer-Tropsch catalysts contain the following: "The invention was made under DOE Contract No. [one of two contracts] and is subject to government rights arising therefrom."

The focus of the work was on the use of the low H_2/CO synthesis gas ratios expected from coal gasification. However, a limited number of runs with a H_2/CO ratio that would be typical of the gasification of natural gas were made.

The work on the preparation, characterization and performance of cobalt and ruthenium catalysts focused on the use of carbonyl clusters with the expectation that these would lead to highly dispersed supported metal catalysts. As part of this study a baseline catalyst was prepared by the "normal" procedure using a cobalt nitrate precursor and aqueous impregnation techniques.

The workers utilized a number of catalyst supports. These included: ?-Al_2O_3 (Catapal SB, 217 m^2/g, 45 Fm), silica (Davison 952, 339 m^2/g, 70 Fm), MgO•3.6SiO_2 (Florisil, 298 m^2/g, 75 Fm) and titania (Degussa P-25, 50 m^2/g, 2 Fm). These supports were used to prepare the catalysts shown in Table IX.1a and IX.1b.

A common impregnation procedure was used to prepare four batches of a catalyst with a formulation of $Co_2(CO)_8$/$Zr(OPr)_4$/Al_2O_3 in which the metal precursor to

support ratio was held constant (3.55-3.81 wt.% Co with the Co/Zr ratio 0.55). This base case catalyst, including one larger batch, exhibited similar activity and product selectivity, showing that the preparative method was reproducible.

The catalysts covered in the patents (IX.4-IX.6) are prepared using a decomposable salt or organic compound of cobalt, iron or ruthenium. One claim is (IX.5):

"1. Method of making a catalyst comprising the following steps:

(a) treating an inert, inorganic metal oxide catalyst base material with a nonaqueous solution of a decomposable salt or organic compound of a group IVB metal and removing said nonaqueous solution;

(b) impregnating the product of Step (a) with a nonaqueous solution of a decomposable salt or organic compound of a Fischer-Tropsch metal catalyst from the group consisting of cobalt, iron or ruthenium, and removing remaining said nonaqueous solution; and

(c) exposing the product of Step (b) to a reducing atmosphere; all while maintaining said material and said products under conditions sufficient to avoid hydrolysis, oxidation, and calcination thereof."

A number of catalyst formulations were prepared by the patented technique. Fischer-Tropsch synthesis activity and selectivity were obtained in a fixed-bed reactor (screening test) and for those formulations exhibiting a high activity in a 1-liter continuous stirred tank reactor. The conditions used for the screening studies were 240-280^{o}C, CO/H_2 feed = 0.55 - 2.0, 300 psig (2.0 MPa) and a space velocity of 1.0-2.0 NL/g cat/hr.

The $Co_2(CO)_8/Zr(OPr)_4/SiO_2$ (3.5% Co, 6.6% Zr) catalyst was found to be the most active system in the slurry reactor and also gave the best liquid fuel selectivity. The Schulz-Flory pattern was found for the products obtained using this catalyst. The bulk activity ranged from 16 to 54 mole syngas/kg cat/hr. The gasoline range (C_5-C_{11}) products accounted for 20 to 45% of the products and the diesel range (C_{12}-C_{18}) products were 17 to 32%. This catalyst was tested in an extended slurry-phase run that achieved 6 months on stream with a 10% loss in activity.

A comparison was made for 4% cobalt Zr-alumina catalysts in which the dominant difference was the cobalt compound used in the preparation of the catalyst: cobalt carbonyl in an organic solvent and cobalt nitrate in aqueous solution. The specific activity of the nitrate derived catalyst is significantly lower that the one derived from the carbonyl compound when the conversion is effected at 240°C is the CSTR (Table IX.2). However, when the conversions are compared at 260°C, there is less difference between the two conversions; one possibility to account for this is that significantly more sintering of the cobalt occurred for the carbonyl derived catalyst at this higher temperature.

The activity of the $Co_2(CO)_8$-based catalysts decreased with changing supports as follows: SiO_2 >> TiO_2 > Al_2O_3 > MgO•SiO_2 (figure IX.1). The Co/TiO_2 catalyst was found to exhibit an unusually high selectivity for C_{3-5} olefins. Zirconium was found to be the better promoter, compared to Ti, for enhancing activity and selectivity, with the optimum Co/Zr ratio being between 0.5 and 1.0.

As the cobalt loading was increased from 4 to 14 wt%, the catalytic activity remained constant and then eventually declined.

The supported Ru catalyst exhibited initially a high activity but the catalyst deactivated rapidly in the slurry reactor. Thus, not much data were obtained with this catalyst.

They found that the following kinetic expression best fitted the data they obtained over a wide range of conversions:

$$-(r_{CO+H_2}) = kC_{H_2}/(1 + k\, C_{H_2O}/C_{CO}C_{H_2}). \qquad [1].$$

However, it was not possible to discriminate with great confidence among the kinetic equations tested during the study.

Catalyst Activation

The activation of supported metal carbonyl catalysts is frequently done by thermal decomposition under vacuum or inert gas atmosphere (IX.8). During the early work at Air Products, catalysts were activated in syngas. To accomplish this the catalyst precursor was heated to 180^{o}C in a nitrogen flow at atmospheric pressure. At 180^{o}C, the flow was switched to the synthesis gas (CO/H_2 = 1) and then heated to the reaction temperature. At the reaction temperature, the pressure was increased to the one used for the synthesis. Later in their work, they compared the impact of activation in pure H_2 or syngas (CO/H_2 = 1). For a 4%Co-zirconia promoted alumina catalyst, they found that the sample activated in hydrogen had a significantly higher activity and higher yield of liquid fuels (figure IX.2a,b; Table IX.3).

Catalyst Promoters

The Air Products work included a comparison of the promotional effects of zirconia and titania for both silica and alumina supports. The titania promoted cobalt catalyst on both alumina and silica supports showed lower catalytic activity than a similar zirconia promoted catalyst. The bulk activity at 240^{o}C for the alumina supported cobalt was 20 % lower with the titania promoter; with the silica supported cobalt this was 40% lower. The titania promoter also produced more methane and light hydrocarbons than the zirconia promoted cobalt catalyst. Similar activity trends were obtained in both the fixed-bed and slurry reactors; however, the differences in the selectivity were less noticeable in the slurry reactor.

Cobalt Metal to Promoter Metal Ratio

In this study the cobalt to promoter ratio for the silica support was conducted with precursors which contained the same level of cobalt but with a variable amount of promoter. Four catalysts were prepared and the compositions are shown below:

Weight % Cobalt	Weight % zirconium	Co/Zr
4.0	4.8	1.2
4.4	2.3	0.53
4.6	0.1	0.15
4.2	0.0	0.0

The effect of the Co/Zr ratio in the gas-phase reactor on the bulk and specific activities for this series are shown in **figures** IX.3 and IX.4. It appears that the optimum ratio for bulk activity occurs at about Co/Zr = 1; however, for the specific activity it occurs at about Co/Zr = 0.5, the base case catalyst ratio. The usage ratio appears to increase as

the zirconium content increases. The base case catalyst provided the highest yield of liquid fuel, C_5-C_{18}.

Three of the catalysts, Zr/Co = 0, 0.53 and 1.9, that were evaluated in the fixed-bed reactor were also evaluated in the CSTR (figure IX.5). Just as in the fixed-bed reactor, the optimum activity was obtained for the base case catalyst with a Zr/Co = 0.53 ratio.

Metal Loading

Metal loadings of 3.5, 11.0 and 14.4 wt.% Co on silica were evaluated. For the base case (3.5 wt% Co) the Zr/Co ratio was 0.53 but this ratio was not used for the catalysts with the higher cobalt loadings. One reason for using the higher Zr/Co ratio for the two higher Co loadings was to be able to make a comparison with the Co/Zr/silica catalyst that is used by Shell Oil for their Shell Middle Distillate Synthesis (SMDS). There was little change in the bulk activity in increasing Co content from 3.5 to 11.0; however, at all temperatures there was a significant decline in activity upon further increasing the Co content to 14.4 wt.% (figure IX.6). Selectivity to liquid fuels declined as the Co loading increased.

Significant increases were observed for the bulk density with increasing Co loadings: 0.394 g/cc for 3.5 % Co, 0.564 g/cc for 11.0% Co, and 0.883 g/cc for 14.4% Co. Thus, as the experiments were conducted in the fixed-bed reactors, the amount of catalyst contained in the 10 cc catalyst volume increased significantly and this may have been a major factor in determining the bulk activity shown in figure IX.6.

In the slurry reactor tests of the 3.5 and 11.0% Co catalysts, the activity at both 240 and 260^{o}C declined as the Co content increased in contrast to the fixed-bed reactor runs (figure IX.7).

Product Selectivity

Satterfield et al. (IX.9) reviewed the literature with respect to product distributions for slurry Fischer-Tropsch reactor operation, particularly with iron catalysts. It was concluded that product hydrocarbon selectivities follow a predicted Anderson-Schulz-Flory (ASF) distribution characterized by the chain growth probability factor, a, and that previously reported deviations are probably due to experimental artifacts. Fixed-bed temperature gradients, insufficient time to reach steady-state, volatilization of certain fractions, and condensation of high molecular weight material are some of the experimental problems that can give misleading selectivity results. These considerations are for deviations which produce chain-limiting Fischer-Tropsch product distributions; most agree that deviations which produce more high-molecular weight products than predicted by ASF are valid (IX.10). Air Products workers sought to avoid the problems previously encountered by their close attention to experimental details, and by determining product distributions over long-term slurry phase operations with good quantitative mass balances (IX.11).

With the fused iron United Catalysts, Inc. C-73 catalyst, a good fit to the ASF distribution was obtained (figure IX.8). However, for slurry catalyst A2 (later shown to be a cobalt-zirconia-silica catalyst) there was an enhanced product deviation from the ASF distribution for the C_{18}-C_{35} region when the catalyst was operated at 2.21 MPa. The effect of pressure in determining this product enhancement can be seen by comparing curves a and b in figure IX.8.

Another catalyst, B, also shows a deviation from ASF (figure IX.9). There was a significant deviation from the ASF distribution for the C_9-C_{25} products when operating with a feed of $H_2/CO = 0.5$. The yield of 67.3 wt% product obtained in the C_9-C_{25}

products represents a 25 wt% increase over what was considered to be the limit of 54.1% imposed by the ASF distribution.

An adequate explanation for these deviations obtained early in the experimental program has not been offered. These and similar catalysts usually provided "standard" ASF distributions based on the data reported. This implies that some experimental operational problem was responsible for this unusual, and highly desirable, deviation from ASF distribution.

Ruthenium Catalyst

A Ru/Zr/alumina ($Co_2(CO)_8$) was a promising catalyst when tested in the fixed-bed reactor. The fixed-bed activity was 26.7 mol syngas/kg cat/hr (comparable to the Co base case catalyst) and a high specific activity of 0.48 mol/mol Ru/min. Methane production was high at about 20%. Slurry phase testing of this catalyst indicated a significantly lower catalytic activity (8 mol syngas/kg cat/hr).

A Ru/Zr/silica catalyst was also tested and it exhibited a much higher activity (70 mol syngas/kg cat/hr; 0.834 mol CO/mole Ru/min at 240^{o}C; 81 mol syngas/kg cat/hr and 1.05 mol Co/mol Ru/min at 260^{o}C) than the similar catalyst using alumina as a support. The Ru catalyst produced higher molecular weight products than a similar Co catalyst. Methane selectivity was low, never exceeding 5.3%.

The performance of the Ru/Zr/silica catalyst was poor in the CSTR. Initially showing a high activity at 240^{o}C (43 moles syngas/kg cat/hr), it had declined to 4 moles syngas/kg cat/hr after only 280 hours on stream.

These preliminary results led the workers to concentrate their further efforts on their cobalt catalysts.

Improving Water-Gas-Shift (WGS) Activity

Since both the Ru and Co catalysts exhibited very low WGS activity, attempts were made to modify the catalyst to increase the WGS activity. A physical mixture of the base case catalyst and a commercial Cu/Zn/alumina low temperature shift catalyst was employed. The addition of the shift catalyst caused a decrease in the Fischer-Tropsch synthesis without increasing the WGS activity. A Co/Fe/alumina catalyst was prepared using the carbonyl compound of Co and Fe. There was a 53% increase in the usage ratio indicating increased WGS; however, the bulk activity declined by 40%. A Fe/Co/Zr/silica catalyst showed only a slight increase (14%) in usage ratio and a slight decrease in bulk activity. Thus, the exploratory effort to increase the WGS activity failed.

Extended Runs in CSTRs

A run of nearly 6 months was made with a Co/Zr/silica catalyst (4.43% Co, 7.58% Zr) (IX.12). This catalyst displayed remarkable stability. During the first 1012 hours it was utilized at 240°C, 300 psig, CO/H_2 = 0.5 and space velocity = 1.8 l/g cat/hr, and then from 1012 to 2188 hours at 260°C, 300 psig, CO/H_2 =1 and space velocity = 2.0 L/g cat/hr. The productivity declined from 52.7 to 46.9 mol syngas/kg cat/hr during 1012 hours (figures IX.10 and IX.11) and then declined slowly during operation from 1012 to 2188 hours (figures IX.12 and IX.13). During the second period the product selectivity remained nearly constant (figure IX.14).

After 2188 hours, a series of changes from the base case conditions, 260°C, 300 psig, space velocity 2.0 L/g cat/hr and CO/H_2 = 1.0, were made for the CO/H_2 ratio and the space velocity to generate data for kinetic studies. At intervals, the conditions were returned to the base case to obtain data to correct for the slow catalyst aging. A series of tests were made at two feed set of conditions. In one instance, the impeller

speed was altered using constant feed conditions and in the other the space velocity was varied by adding a nitrogen flow, maintaining the same partial pressure of hydrogen and carbon monoxide by increasing the total pressure. Both variations show that mass transfer effects can be neglected.

At 3964 hours, the temperature was increased to 280^{o}C to repeat the series of kinetic measurements. At this temperature the methane production was very high (up to 56.4%) and the wax production very low. At the end of the experiment, the reactor contained only solid, indicating that the operations at the higher temperature had caused the reactor to loose essentially all of the liquid through vapor pressure and/or hydrogenolysis effects.

Cobalt Dispersion

Hydrogen chemisorption was measured to obtain a measure of the metal dispersion of the cobalt and ruthenium catalysts. Air Products reports indicate that they were disappointed with the low dispersions that they obtained; however, the 10-12% dispersion values they obtained for 11 and 14% Co on silica are about as high as reported by later workers. In general, the silica supported Co exhibited a higher dispersion than the alumina supported cobalt at a similar metal loading (**Table** IX.4). The hydrogen chemisorption was considered to decrease along with the catalytic activity as the cobalt loading was increased for the silica supported cobalt catalysts. The dispersions obtained by the Air Products workers agree with those reported by Reul and Bartholomew (IX.13). Chemisorption was measured at higher temperatures because this led to higher surface areas.

Olefin Reincorporation

In a screening study, ethene was added to the syngas feed for runs with the $Co_2(CO)_8/Zr(OPr)_4/Al_2O_3$ catalyst (5.07% Co; 4.39% Zr). Under the reaction conditions employed, the CO conversion should have been 20% or less. When 10 or 20 volume percent ethene was added to the feed, the major result was the production of ethane. The oxygenate production did increase slightly (from 0.2 to 2.4 wt%) but the majority of this fraction was propanol, the product of hydroformylation. The catalyst underwent significant (20% conversion) deactivation during the addition of ethene. The conclusion is that ethene did not undergo significant incorporation; rather it was hydrogenated to ethane.

Kinetic Study

A program was developed to obtain kinetic data from the experimental data (figure IX.15). Experimental data from two runs were made with a catalyst formulation that was essentially the same as the base case catalyst but a more active $Co_2(CO)_8/Zr/SiO_2$ catalyst (4.9% Co; 9.3% Zr). Henry's Law was assumed to apply and to allow for calculation of vapor partial pressures. Henry's Law data was taken from Peter and Weinert (IX.14) and liquid densities were calculated using correlations proposed by Deckwer (IX.15). Mass transfer from bulk liquid to catalyst surface was considered to negligible, based upon the experimental data.

The authors fit the data to five kinetic expressions (to correlate with equations in reference 13, A=2, B=1, C=3, D=4):

$$-r_{CO+H_2} = k\, C_{H_2}/(1 + KC_{CO_2}/C_{CO}) \quad [2]$$

$$-r_{CO+H_2} = k\, C_{H_2}/(1 + KC_{H_2O}/C_{CO}) \quad [3]$$

$$-r_{CO+H_2} = k\, C_{H_2}/(1 + K_1C_{CO_2}/C_{CO} + K_2C_{H_2O}/C_{CO}) \quad [4]$$

$$-r_{CO+H_2} = k\, C_{H_2}/(1 + KC_{H_2O}/C_{CO}C_{H_2}) \quad [5]$$

$$-r_{CO+H_2} = kC_{H_2}^{a} C_{CO}^{b}. \quad [6]$$

For the run with the catalyst similar to the baseline catalyst, the data at high H_2/CO feed ratios and at high space velocities were best described by the first order rate equation:

$$-r_{CO+H_2} = kC_{H_2}^{a} C_{CO}^{b}. \quad [7]$$

where a = 1.1 and b = 0. For low H_2/CO data, equation 3 fits the data better:

$$-r_{CO+H_2} = k\, C_{H_2} / (1 + KC_{H_2O} / C_{CO}) \quad [8]$$

where k = 0.349 and K = 0.425. The activation energy was in the range of 33-44 kJ/mole.

For the more active catalyst, none of the five equations were able to be used to fully describe the data. They concluded that equation 3 provided the better fit to the data and transformed the equation to a linear form:

$$C_{H_2} / -r_{CO+H_2} = (K/k)\, C_{H_2O} / C_{CO} + (1/k). \quad [9]$$

The data are plotted using equation 7 and is shown in figure IX.16 for 240, 260 and 280°C. From the intercept, the rate constant, k, is derived with values ranging from 0.328 to 0.775 cc/g cat/sec. This allows K to be determined from the slope and values ranging from 0.466 to 0.302 are obtained. An activation energy of 51 kJ/mole was obtained from the Arrhenius plot.

The authors write that, at that time, relatively few kinetic studies of the Fischer-Tropsch reaction using cobalt catalysts have been made (IX.17-IX.22). From the available literature, activation energies for cobalt catalysts are in the range of 67-117 kJ/mole; for iron catalysts they range from 37 to 105 kJ/mole. The activation energies obtained by the Air Products workers for these catalysts are surprisingly low.

The Air Product workers analyzed the kinetic data obtained during run hours 2188 and 3964 in the extended run described above. It was assumed that the deactivation led to a linear decrease in conversion during the kinetic measurements. They concluded that Equation 5, which included water inhibition, fit the data better than the other equations; a plot of the data using the linearized form of Equation 5 is shown in figure IX.17. It had been reported by Huff and Saterfield (IX.23) that this equation describes data with high water concentration quite well. After Equation 5, the data was best fit by equation 6. The rate constant obtained using Equation 5, based upon fresh catalyst activity, are $K = 5.24 \times 10^{9} \exp(-23{,}254/RT)$ cc/g cat/sec and $K = 1.55 \times 10^{-3} \exp(-6{,}250/RT)$ mol/cc. The Arrhenius plot returned an activation energy of 97 kJ/mole, and this value agrees much better with those reported earlier for cobalt catalysts.

Slurry Reactor Hydrodynamics Studies

The final report (IX.24) provides a detailed summary of the literature to that date (about 1983) and experimental data obtained in cold flow simulators of 12.7 and 30.5 cm diameter (1.52 and 4.75 m height, respectively) that was conducted at Air Products. With the simulator, phase holdups, phase dispersion coefficients, and interphase heat and mass transfer coefficients were measured. The measured heat and mass transfer and phase dispersion correlations were found to conform to the literature, while the phase holdup correlations were different from the literature. The product distributions from Air Products' catalyst testing program were combined with the hydrodynamic studies to make predictions of space-time yields of product fuel fractions in large-scale bubble column reactors.

Based upon the study, they concluded:

1. Both hydrodynamic and kinetic effects are important to the proper design of the bubble column reactor.
2. For solid particles below 60 Fm, the slurry can be modeled as a pseudo-single phase. Larger size solid particles were distributed in accordance with Cova's sedimentation-diffusion model (IX.25).
3. Of those studied, the most important independent variable affecting the reactor performance was the superficial gas velocity, followed by solid particle loading. The type of liquid had a small effect on the column hydrodynamics. The parameters that had little or no effect in the range studied included the presence of heat transfer internals, solid type, distributor hole size, and superficial slurry velocity.
4. Staging the bubble column system to provide more plug flow behavior of the gas was predicted to result in a 5% increase in conversion rates, assuming the same bubble size, about 0.23 cm, as in the unstaged column. On the other, if the average bubble diameter is decreased to 0.07 cm, the conversion rates are expected to increase by 25%.
5. The gas holdup obtained in the cold flow systems was lower than measured by Deckwer (IX.26) and Mobil (IX.27) but in agreement with results of Satterfield (IX.28) and with the correlations from Air Products' slurry phase methanol project (IX.29).
6. Adding seven, 5.7 cm o.d. x 1.42 m heat transfer internals to the 30.5 cm column had no effect on column hydrodynamics.
7. The heat transfer results agreed with Deckwer's correlation (IX.30) but, unlike Deckwer, the heat transfer rates continued to increase beyond a 10 cm/s

superficial gas velocity. Heat transfer tubes would therefore take only a small fraction of the internal volume of a Fischer-Tropsch slurry bubble column reactor.

8. Mass transfer results agreed with Akita and Yoshida (IX.31) and Hikita et al. (IX.30-IX.33).

9. Liquid dispersion results agreed with Kato et al. (IX.34), indicating that above a superficial gas velocity of 3 cm/s, the slurry was well-mixed.

The Air Products workers wrote, "One of the more important aspects of gas flowing through a tubular reactor is its availability at the reaction site. This is ultimately related to the interfacial area between the liquid and gaseous phases. In a two-phase, gas-liquid system, the interfacial area, a, is related to the gas volume fraction, e_G, and mean bubble size, d_{SB}, by

$$a = 6\, e_G / d_{SB} \qquad [10]$$

Both the mean bubble size, also known as the Sauter mean diameter, and the volume fraction, which is typically referred to as gas holdup or void fraction, are values which are extremely important to optimum reactor design."

The Air Products work followed three steps:

1. Hydrodynamic data were obtained in a 5" ID x 5' (12.7 cm ID x 1.52 m) cold flow simulator.

2. Scale hydrodynamic study to 12" ID x 15.5' (30.5 cm ID x 4.75 m) column.

3. Incorporate kinetic data from catalyst studies with hydrodynamic correlations into a computer model and use this to predict the conversion rates and space-time yields that would be obtained in actual Fischer-Tropsch slurry reactor

operation. Using the model, the heat, mass and momentum transfer parameters which most affect the bubble column design were better quantified.

In the slurry reactor, either mass transfer resistance or kinetic resistance is expected to dominate. Gas holdup, average bubble size and mass transfer coefficient are the important dependent variables that impact mass transfer resistance. Two important factors for kinetic resistance are solids dispersion and liquid dispersion, both affecting catalyst loading, and thereby reactor productivity. Heat transfer rate is also important since this will determine the fraction of the reactor volume required for heat exchangers, and not available for production. The Air Products work attempted to quantify the above mentioned parameters (Table IX.5).

The workers reviewed work prior to 1982 concerning gas-liquid-solid systems. They indicate that Kara (IX.35) found that solid particles promote bubble coalescence and hence the onset of the churn-turbulent regime. However, reports of solids decreasing or increasing gas-holdup can be found in the literature. Kurten and Zehner (IX.36) report Sittig's work on bubble breakup caused by solids. It was shown that bubble breakup occurs when the inertia forces of the solid particle exceed the bubble surface tension forces:

$$(p/6)(?_S/2)\, d_S^3\, u_{SG}^2 > (p/4)\, s\, d_S^2 \qquad [11]$$

which, when rearranged, shows that bubble breakup can occur when the Weber number is greater than 3:

$$We = (?_S\, d_S\, u_{SG}) / s \ \$ 3 . \qquad [12]$$

This indicates that below the critical Weber number the solid will not cause bubble breakup.

Since for a particle of about 4 or about 100 Fm, a bubble rise velocity > 0.1 or 0.65 m/sec, respectively, is needed for the particle to induce bubble breakup, it is not anticipated that Fischer-Tropsch slurry column will experience bubble breakup due to the presence of solid catalyst particles. In fact, it is expected that bubble coalescence will occur, decreasing gas holdups.

Deckwer et al. (IX.15) studied gas holdup in 4.1 and 10 cm ID columns in the bubbly flow regime (1 to 4 cm/sec) using a hydrogenated Fischer-Tropsch liquid and up to 16 wt.% of > 5 micron alumina particles and obtained the empirical correlation:

$$e_G = 0.053\ j_G^{1.1} \qquad [13]$$

where j_G is the superficial velocity of the gas. It was suspected that foaming occurred in the measurements reported by Deckwer et al. (IX.15). Kuo (IX.27) obtained data for the same system showed that with a sintered plate gas distributor he obtained foaming but that no foaming and a much smaller gas holdup was obtained with a distributer with larger openings. Bukur (IX.37) used the same wax as Deckwer and Kuo and obtained a means of eliminating the formation of a foam region. In the absence of a foam region, Bukur obtained a gas holdup that was comparable to those of Pilhofer and Bach (IX.38) and the results obtained by Air Products.

It was concluded that gas holdup was mostly a function of gas velocity and varies to the first power. Slurry density, or weight loading, has the second largest impact on gas holdup. The larger column (30.5 cm) had a lower gas holdup than the 12.7 cm column at the higher gas velocities. It was considered that this was due to more bubble coalescence in the taller column and that the data obtained in the larger diameter column, being more reliable, would be used in the computer simulation of an operating commercial Fischer-Tropsch reactor.

The gas bubble diameter was obtained over a wide range of conditions. The bubble diameter, d_{SB}, relationship with the gas holdup, the gas liquid interfacial area is related to the Sauter mean bubble diameter and gas holdup by

$$a = 6\, e_G / d_{SB} \,. \qquad [14]$$

The uncorrected bubble chord lengths were in the range from 0.28 to 0.44 cm. The measured values are slightly larger than the true values because the experimental approaches caused bubble acceleration/elongation during the measurement. The corrected bubble diameters ranged from 0.22 to 0.35 cm and the bubble velocity ranged from 26.3 to 32.7 cm/sec, both range over fairly narrow values. Since the bubble size should be smaller in Fischer-Tropsch liquids than in water, they concluded that the Calderbank (IX.39) correlation suggested a Sauter diameter size of 0.23 cm for a Fischer-Tropsch type system and this produces

$$a = 6\, e_G / 0.23 = 26.09\, e_G \qquad [15]$$

which was used in the computer model.

The overall mass transfer coefficient, K_La, is the product of the mass transfer rate per unit area, K_L, and the interfacial area, a. Air Products workers measured K_La because of the variation in the reported values. This variation was primarily due to variation in the reported gas holdup and average bubble size; however, there is also variation in the reported values of K_L. They obtained an empirical correlation for K_La:

$$K_La = (0.30\, e_G^{1.06}\, d_p^{0.05}) / W^{0.08} \qquad [16]$$

where W = weight fraction of solids. Gas velocity was considered to be the primary factor in estimating K_La.

Liquid dispersion relates to how well mixed the liquid phase is and how much solid can be suspended. The Air Products workers discussed this in terms of two extremes:

1. Ideal mixing, continuous stirred tank reactor (CSTR) behavior where any liquid molecule can move to any other part of the column from one instant to the next, and
2. Plug flow reactor (PFR), where any molecule will move in concert with the other neighboring molecules, entering and leaving the column at the same time.

The axial liquid dispersion coefficient, E_z, provides one was to quantify where a particular reactor lies between these two extremes (CSTR and PFR). E_z will be zero for PFR and infinity for CSTR behavior. In practice, when E_z is greater than 10^{-2} m^2/sec, a well-mixed behavior exists. Knowing E_z, one can plot a sample's concentration as a function of time at a fixed point within the column; such a plot is a residence time distribution (RTD) curve.

A model that is used to describe the sample concentration at any time is Fick's Law:

$$dC/dt = E_Z \, d^2C/dZ^2 \, . \qquad [17]$$

Using the appropriate boundary conditions, an approximate analytical solution which describes the RTD curve at any point within the column was given by Ohki and Inoue (IX.40):

$$dC/dt = E_L \, d^2C / dZ^2. \qquad [18]$$

For the boundary conditions where a tracer impulse is inserted at any longitudinal location:

$$dC/dt)_{0,T} = dC/dZ)_{L,T} = 0 \qquad [19]$$

where L = extended bed height and

$$C(Z,O) \;=\; \begin{cases} O, & O \le Z < Z_1 \\ C_O, & Z_1 \le Z \le Z_2 \\ O, & Z_2 < Z \end{cases} \qquad [20]$$

$$C/C_e \;=\; 1 - 2 \sum_{n=1}^{100} [\cos(n\pi Z/L)\exp(-n^2\pi^2 E_L t/L^2)] \qquad [21]$$

Little difference is obtained if the summation is to infinity, the exact solution, or stops at 100.

The experimental program to address the dispersion issue and to obtain the RTD curve utilized the injection of a sodium chloride solution into water, detecting the movement of the sodium chloride, the tracer, by conductivity measurements at various heights in the column.

The energy dispersion is greatest at the gas distributor inlet and least at the gas disengagement zone at the top of the reactor. However, E_Z was not height dependent was not evident since one dispersion coefficient was sufficient to characterize the entire column. The results of the liquid dispersion runs at Air Products were in agreement with the work of Kato and Nishiwaki (IX.41):

$$Pe = (13\ Fr) / (1 + 6.5\ Fr^{0.8}) \qquad [22]$$

where Pe is the Peclet number $((V_G\ d_C) / E_Z)$ and Fr is the Fraud Number $(V_G / g\ d_S)^{1/2}$.

From their experimental work, they obtained data to show that a uniform distribution of 0.5-5 micron sized particles was obtained. With larger particles there was, as expected a distribution of particles along the column height, with more at the bottom than the top. They concluded that nonagglomerating catalyst particles less than 60 microns should be suitable for Fischer-Tropsch bubble column batch operation, as no unsuspended solids were observed.

Heat transfer was studied by placing tubes with heaters in the bubble column. It was noted that the agitation produced by the gas phase within the reactor produces heat transfer coefficients that are higher than those produced by gas or slurry alone. The heat transfer surface needed for internal use is less than required for an external exchanger.

The report ends with an engineering evaluation that utilizes the model proposed by Deckwer et al. (IX.42). The substitution of the Air Products correlations for those in Deckwer's model showed little effect at low gas velocities. At 9 cm/sec the space-time yield was doubled (Tables IX.6 and IX.7). A major reason for this was that the lower gas holdup allowed for more catalyst per unit volume. In the bubble column operation there exists an optimum gas holdup which will maximize column space-time yield. Gas holdups higher than this optimum will be reaction rate-limited while those lower than this will be mass transfer-limited. The optimum gas holdup will be affected by the bubble size (b_{SB}), intrinsic kinetic rate (K_o), catalyst weight loading (W), the rate of mass transfer across the gas-liquid interface (K_L), and the usage ratio (U). The optimum gas holdup is given by the expression:

$$a\ opt = 1 / [1 + (6\ K_L(1 + U) / K_o W d_{SB})^{1/2} . \qquad [23]$$

Using this equation allows one to calculate the relative space-time yields for a variety of K_o, W and D_{SB} (Table IX.8).

The Air Products workers compared the space-time yield for a bubble column reactor and for a series of staged reactors. In the first method of calculating the space-time yield, a number of idealized CSTRs are simulated with almost complete recycle of the liquid and catalyst but no recycle of the gas phase. This model would be equivalent to the recirculating cell model used in the literature. In the second method,

the extent of backmixing of the gas phase was modeled by applying an axial dispersion model (IX.43).

In this model, a low dispersion coefficient refers to many CSTRs in series, while a high dispersion coefficient refers to very few CSTRs in series. Carberry (IX.44) showed that the two methods are relates so that:

$$N = V_G L/2D \ . \qquad [24]$$

Since the Deckwer computer model incorporates the axial dispersion model for the gas, liquid and catalyst phases, this approach was chosen.

Results of simulating the Rheinpreussen-size column as several stages as having the same total volume as the original single-stage column (figure IX.18) are shown in Table IX.9. Thus, a 5% increase in space-time yield is obtained by using 5 CSTRs but a further increase does not lead to a further increase in yield (figure IX.19).

Design of LaPorte Plant

As part of the work, a design for a pilot plant to be located at La Porte, Texas adjacent to an Air Products plant was completed (IX.45). The bubble Fischer-Tropsch reactor was sized to operate in the churn-turbulent flow regime, in which commercial-scale reactors will operate. The study indicated that this flow regime could be achieved with an effective reactor diameter of five inches. However, it was recognized that the exact diameter of the transition from the quiescent to churn turbulent regime is an unknown function of the slurry viscosity and surface tension. To achieve a 40-50% conversion of the synthesis gas in a single pass at a superficial gas velocity of 0.3 ft/sec would require a 30 foot expanded slurry height.

The reasons for the choice of flow regime were described. Concurrent up-flow bubble columns can operate in any one of three flow regimes (IX.15) and these are

illustrated in figure (IX.20) together with an indication of the Air Products cold flow work, the LaPorte design and the Rheinpruessen work. The bubbly flow or quiescent regime occurs at velocities less than typically 0.15 ft/sec. Bubbles are of uniform size and do not interact or coalesce to any substantial degree. At higher velocities, the bubbles do not rise uninfluenced by neighboring bubbles and the churn turbulent regime is entered. Coalescence occurs, yielding larger bubbles and faster rise velocities. Because of coalescence, gas holdup does not increase as quickly with gas flow rate in the churn turbulent regime as in the bubbly flow regime. Where the coalesced bubble would be larger than the diameter of the column, the slug flow regime is reached. Slug flow is undesired because of the low gas/liquid interfacial area and the tendency for the slurry to be lifted out of the reactor along with the gas.

The choice of flow regime was dictated by two economic factors. For a given reactor volume:

1. The highest space time yield or production rate per unit volume is optimal.
2. A tall column is preferred to a short one.

The higher the space-time yield, the smaller the reactor volume required for a given production. The simulations with the Deckwer model and the Air Products hydrodynamic and catalytic data showed that, in every case, the optimum gas velocity for a maximum space-time yield falls within the churn turbulent regime. It was concluded that the value of 9.1 cm/sec (0.3 ft/sec), although slightly below the optimum, would still allow a reasonable conversion for the reactor height chosen.

Air Products workers wrote, "For a commercial plant with multiple trains, it is advantageous to have as few reactor vessels as possible. In the quiescent regime only about 15' of reactor height is required to achieve 90+% conversion of syngas. By

increasing the gas velocity into the churn turbulent regime, 90+% conversion of syngas is not achieved until a height of 60'. For equivalent STY's, it is more economical to have N vessels at 60' than to have four times that number of vessels, each with a height of 15'." (IX.45).

The slurry reactor was designed to operate in a fluidized-bed mode. Once charged, the slurry will not be added or removed except for removal of high molecular weight products that form during reactor operation. Gas will flow up the column and exit out the column top.

The design was implemented at the La Porte location and the plant has been modified during the years of operation. To date, four runs, two with an iron catalyst and two with cobalt catalyst, have been conducted.

References

IX.1. Novel Fischer-Tropsch Slurry Catalysts and Process Concepts for Selective Transportation Fuel Production; DOE/PC/70030; Reports T1 through T9; Final Report: H. P. Withers, Jr, K. F. Eliezer and J. W. Mitchell, Novel Fischer-Tropsch Slurry Catalysts and Process Concepts for Selective Transportation Fuel Production; DOE/PC/70030-T9, December 1987.

IX.2. Catalyst and Reactor Development for a Liquid-Phase Fischer-Tropsch Process; DOE/PC/30021, reports T4 through T22.

IX.3. Development and Process Evaluation of Improved Fischer-Tropsch Slurry Catalysts; DOE/PC/80011, Reports T1 through T-11; Work done at Texas A&M University, March 1987 through April 1990.

IX.4. P. N. Dyer, R. Pierantozzi and H. P. Withers, Supported Fischer-Tropsch catalyst and method of making the catalyst, US 4,681,867, July 21, 1987.

IX.5. P. N. Dyer and R. Pierantozzi, Catalyst for selective conversion of synthesis gas and method of making the catalyst, US 4,619,910, Oct 28, 1986.

IX.6. P. N. Dyer, R. Pierantozzi and H. P. Withers, Fischer-Tropsch process, US 4,670,472, June 2, 1987.

IX.7. E. B. Cornelius and D. W. Koester, Particles featuring gamma alumina, US 3,669,904, June 13, 1972.

IX.8. J. Swart and R. Snel, J. Mol. Catal., 30, 305 (1985).

IX.9. C. N. Satterfield, G. A. Huff and J. P. Longwell, Ind. Eng. Chem. Proc. Des. Dev., 21, 465 (1982).

IX.10. B. H. Davis, ACS Div. Fuel Chem. Preprints, 37, 172 (1992).

IX.11. J. V. Bauer, B. W. Brian, S. A. Butter, P. lN. Dyer, R. L. Parsons and R. Pierantozzi, "Catalytic Conversion of Synthesis Gas to Alcohols and Chemicals," (R. G. Herman, Ed.) Plenum, New York, 1984, pp. 129-149.

IX.12. H. P. Withers, Jr., K. F. Eliezer and J. W. Mitchell, Ind. Eng. Chem. Res., 29, 1807 (1990).

IX.13. R. C. Reul and C. H. Bartholomew, J. Catal., 85, 63, 78, (1984).

IX.14. S. Peter and M. Weinert, ZZ. Phys. Chem. (Frankfurt), 5, 114, (1955).

IX.15. W. D. Deckwer, et al., Ind. Eng. Chem., Process Des. Dev., 19, 699 (1980).

IX.16. W. D. Deckwer, R. Kokuun, E. Sanders and S. Ledakowicz, Ind. Eng. Chem., Process Des. Dev., 25, 643 (1986).

IX.17. M. A. Vannice, J. Catal., 37, 449 (1975).

IX.18. M. A. Vannice, J. Catal., 50, 226 (1977).

IX.19. S. Weller, J. Am. Chem. Soc., 69, 2432, (1947).

IX.20. P. K. Agrawal, J. R. Katzewr and W. H. Manogue, J. Catal., 69, 312, (1981).

IX.21. P. K. Agrawal, J. R. Katzewr and W. H. Manogue, Ind. Eng. Chem. Fundam., 21, 385 (1982).

IX.22. C.-H. Yang, F. E. Massoth and A. G. Oblad, Adv. Chem. Ser., 178, 35 (1978).

IX.23. G. A. Huff and C. N. Satterfield, Ind. Eng. Chem., Process Des. Dev., 23, 696 (1984).

IX.24. Slurry Reactor Hydrodynamics Studies, Final Report, DOE/PC/30021--T20, 151 pp.

IX.25. D. R. Cova, Ind. Eng. Chem. Proc. Des. Dev., 5, 20, 1966.

IX.26. W.-D. Deckwer, "Access of Hydrodynamic Parameters Required in the Design and Scale-up of Bubble Column Reactors, "Reprint from ACS Symposium, No. 168, 1981.

IX.27. J. Kuo, Quarterly Technical Progress reports, US DOE/PC/30022, 1980-1983.

IX.28. C. N. Satterfield and G. Huff, Chem. Eng. Sci., 35, 195 (1980).

IX.29. P. N. Dyer, R. Pierantozzi, B. W. Brian and J. V. Bauer, Quarterly Technical Progress Reports 1-8, US DOE PC/30021, 1980-1983.

IX.30. W.-D. Deckwer, Y. Louisi, A. Zaidl and M. Ralek, Ind. Eng. Chem., Proc. Des. Dev., 19, 699, 1980.

IX.31. K. Akita and F. Yoshida, Ind. Eng. Chem. Process Des. Dev., 12, 76 (1973).

IX.32. H. Hikita and H. Kikukawa, Chem. Eng. J., 8, 191, (1974).

IX.33. H. Hikita, S. Asal, K. Tanigawa, K. Segawa and M. Kitau, Chem. Eng. J., 22, 61 (1981).

IX.34. Y. Kato and A. Nishiwaki, J. Chem. Eng. Japan, 5, 112 (1972).

IX.35. S. Kara, G. Balmuhan, B. G. Kelkar, Y. T. Shah and N. L. Carr, Ind. Eng. Chem. Proc. Des. Dev., 21, 584, (1982).

IX.36. H. Kürten and P. Zehner, German Chem. Eng., 2, 220, (1970).

IX.37. D. B. Bukur, preliminary results communicated to Air Products, 1985.

IX.38. T. H. Pilhofer, H. F. Bach and K. H. Mangartz, ACS Symp. Ser., 65, 372, (1978).

IX.39. P. Calderbank, et al., "Catalysis in Practice," Symp. Proceed. Instr. Chem. Eng., 1963, p 66.

IX.40. Y. Ohki and H. Inoue, Chem. Eng. Sci., 25, 1, (1970).

IX.41. Y. Kato and A. Nishiwaki, Intl. Chem. Eng., 12, 182 (1972).

IX.42. W. D. Deckwer, Y. Serpemen, M. Ralek and B. Schmidt, Ind. Eng. Chem. Proc. Des. Dev., 21, 231 (1982).

IX.43. O. Levenspiel, "Chemical Reaction Engineering," John Wiley & Sons, Inc., 1972, p 310.

IX.44. J. J. Carberry, "Chemical and Catalytic Reactor Engineering," McGraw Hill Book Co., New York, 1976, p 163.

IX.45. "Catalyst and Reactor Development for a Liquid Phase Fischer-Tropsch Process, Final Report for Task 4, DOE/PC/30021-T22.

Table IX.1a.

Compositions (wt.% of catalyst) and specific catalytic activity (mol CO/mol metal/min) for catalysts prepared using an alumina support during the Last Three-Year DOE Contract (reference IX.1).

Co	Zr	Ti	K	Fe	Mn	Act.
3.6	6.6					0.25
4.4	1.8					0.31
3.4	6.6				1.6	0.31
2.8	4.9					0.48
1.4				0.51		0.40
1.2			0.3	0.4		
4.7[a]						0.25
3.5		8.6				0.23
2.6				0.85		0.34
2.4			0.02	0.79		0.27
3.9	5.0					0.24
5.1[a]	4.4					0.20
4.2[a]	7.1					0.20
4.0	6.4					0.21
10.8	8.5					0.26
3.5	6.6					0.51
3.7	7.3			0.72		0.26

a. Cobalt added as cobalt nitrate.

Table IX.1b.

Compositions (wt.% of catalyst) and specific catalytic activity (mol CO/mol metal/min) for catalysts prepared using an silica support during the Last Three-Year DOE Contract (reference IX.1).

Co	Zr	Ti	K	Fe	Mn	Act.
4.4		4.0				0.24
3.7	7.2					0.23
4.6	7.5					0.43
4.0	3.3					0.83
3.5						0.31
	7.3			2.4		n.d.
4.0	4.8					0.44
4.4	2.3					0.32
4.6	2.3					0.32
4.2						0.14
4.1	6.8					0.31
11.0	7.4					0.15
14.4	10					0.07

Table IX.2

Effect of Co source on activity and selectivity of 4% Co on Zr/alumina catalyst tested in the slurry phase using a CSTR at 300 psig, CO/H_2 = 1.0 and 2.0 NL/g cat-hr. (from reference IX.1)

Cobalt Source	Carbonyl	Carbonyl	Nitrate	Nitrate
	240°C	260°C	240°C	260°C
Bulk activity, mol syngas/kg cat/hr	35.3	38.5	15.8	29.9
Specific activity, mol CO/mol Co/min	0.29	0.32	0.09	0.21
Selectivity, Wt.%				
C_1	7.9	10.4	10.9	16.5
C_{2-4}	13.7	15.0	6.5	11.1
C_{5-11}	37.0	44.5	12.9	26.5
C_{12-18}	23.4	25.8	19.8	23.8
C_{19-23}	8.9	2.0	21.9	10.6
$C_{24}+$	9.1	2.3	28.0	11.5
TOTAL FUELS, C_{5-23}	69.3	72.3	54.6	60.9

Table IX.3

Effect of syngas vs. hydrogenation activation on the activity and hydrocarbon selectivity using a 4% Co on Zr/Al_2O_3 catalyst in a slurry CSTR (from reference IX.1)

	Syngas	H_2
Space velocity, NL/gcat/hr	1.6	2.0
CO/H_2	1.6	1.5
Pressure, psig	300	300
Temperature, ^oC	250	258
Hydrocarbon, wt.%		
C_1	11.5	7.2
C_{2-4}	10.4	10.8
C_{5-11}	29.2	34.1
C_{12-18}	15.3	27.9
C_{19-23}	12.5	8.6
$C_{24}+$	21.1	11.4
C_{5-23}	57.0	70.6

Table IX.4

Metal dispersion for Co and Ru Catalysts (from reference IX.1)

Catalyst	BET Surface Area, m^2/g	Metal Surface Area, m^2/g	Dispersion, %
3.5%Co/Zr/SiO_2	316	1.9 (a)	6
4.0%Co/Zr/Al_2O_3	209	0.3 (b)	1
4.1%Co/Zr/SiO_2	210	1.9 (a)	7
11.0%Co/Zr/SiO_2	302	8.1 (a)	12
10.8%Co/Zr/Al_2O_3	n.d.	5.4 (a)	7
14.4%Co/Zr/SiO_2	145	9.3 (a)	10
4.0%Ru/Zr/SiO_2	325	1.6 (b)	8

(a) Hydrogen chemisorption performed at 100°C
(b) Hydrogen chemisorption performed at 35°C.

Table IX.5

Slurry Reactor Design Variables Considered in the Air Products Study (reference IX.21)

DEPENDENT VARIABLES	
Gas Hold-Up	Mass Transfer
Bubble Size	Liquid Dispersion
Solids	Heat Transfer
INDEPENDENT VARIABLES	
Slurry Medium: Paraffin, water	
Superficial Gas Velocity: 1.52 - 15.2 cm/sec	
Superficial Slurry Velocity: 0 - 3.0 cm/sec	
Solid: Silica, Iron Oxide	
Solid Size: 1 - 5 Fm, 45 - 53 Fm, 90 - 106 Fm	
Solid Concentration: 0, 10, 20, 30 Wt.%	
Distributor Hole Size: 0.9, 3.2, 12.8 mm	
Heat Transfer Internals: None, Plain	

Table IX.6

Rheinpreussen Simulation using Deckwer Correlations (from reference IX.1)

REGIME	CHURN TURBULENT		
CATALYST	Base Case	Cat. A	Cat. B
Inlet gas velocity, cm/sec	9.00	9.00	9.00
Gas holdup	0.385	0.512	0.526
Interfacial area, cm^2/cm^3	32.66	43.44	44.66
Temperature, ^oC	260.2	259.7	260.2
Rate Constants			
Preexponential factor (sec wt.% in slurry) x 10^5	1.12	90.3	115
Activation energy, kJ/mol	70	94.7	94.7
Inlet ratio, mol CO/mol H_2	1.5	1.5	1.98
Usage ratio, mol CO/mol H_2	1.5	1.5	0.65
Hydrogen conversion, %	80.4	34.9	49.8
Relative mass transfer resistance	0.106	0.021	0.035
Space-time yield, mol CH_2/hr	2937	1065	1022
Constants in Case Study			
Reactor length, ft (cm): 26.25 (800)			
Reactor diameter, in (cm): 59 (150)			
Contraction factor: -0.5			
Particle diameter, Fm: 50			
Reactor pressure, psig (bar): 174 (12)			
Weight fraction catalyst in slurry: 0.20			
Specific heat transfer area, cm^2/cm^3: 0.10			

Table IX.7

Rheinpreussen Simulation using Air Products Correlations (from reference IX.1)

REGIME	CHURN TURBULENT			
CATALYST	Base Case*	Cat. A	Cat. B#	Cat. B with Shift
Inlet gas velocity, cm/sec	9.00	9.00	9.00	9.0
Gas holdup	0.385	0.149	0.171	0.146
Interfacial area, cm^2/cm^3	32.66	36.06	41.43	35.39
Temperature, ^oC	260.2	260.4	260.4	261.1
Rate Constants				
Preexponential factor (sec wt.% in slurry) x 10^5	1.12	90.3	115	115
Activation energy, kJ/mol	70	94.7	94.7	94.7
Inlet ratio, mol CO/mol H_2	1.5	1.5	1.98	1.98
Usage ratio, mol CO/mol H_2	1.5	1.5	0.65	1.98
Hydrogen conversion, %	80.4	55.9	62.9	58.5
Relative mass transfer resistance	0.106	0.043	0.069	0.048
Space-time yield, mol CH_2/hr	2937	2042	1273	2135
Constants in Case Study				
Reactor length, ft (cm): 26.25 (800)				
Reactor diameter, in (cm): 59 (150)				
Contraction factor: -0.5				
Particle diameter, Fm: 50				
Reactor pressure, psig (bar): 174 (12)				
Weight fraction catalyst in slurry: 0.20				
Specific heat transfer area, cm^2/cm^3: 0.10				

*Operating conditions at Rheinpreussen
#Cold flow model gas holdup correlation

Table IX.8

Optimum gas holdup, gas velocity*, and space-time yield (STY) (K_L = 0.0205 cm/s; U = 2) (from reference IX.1)

CASE	K_o, sec^{-1} $wt\%^{-1}$	W, %	d_B, cm	a opt, vol %	V_G cm/sec	STY
1	$1.4x10^{-3}$	20	0.07	6.8	2.13	1.00
2	$1.4x10^{-3}$	60	0.07	11.2	12.75	2.72
3	$6.1x10^{-3}$	60	0.07	20.9	36.43	9.42
4	$1.4x10^{-3}$	20	0.30	13.1	5.29	0.87
5	$1.4x10^{-3}$	60	0.30	20.7	36.00	2.17

*Using Air Products cold flow gas holdup correlation

Table IX.9

Rheinpreussen simulation for staged reaction systems (from reference IX.1)

NUMBER OF STAGES	1	20	5	20
DISPERSION COEFF., cm^2/s	72.130	128.8	572.5	143.8
Gas Holdup	0.145	0.148	0.158	0.158
Interfacial area, cm^2/cm^3	4.148	12.717	4.514	4.527
Hydrogen Conv., %	66.1	85.1	69.2	69.2
Rel. Mass Transfer Resistance	0.556	0.310	0.542	0.541
Space-Time Yield, mol CH_2	2,417	3,128	2,529	2,530
Improvement Ratio	1.000	1.294	1.046	1.047
CONSTANTS IN CASE STUDY				
Reactor Length, ft (cm): 26.25 (800)				
Reactor Diameter, in (cm): 59 (150)				
Contraction Factor: -0.5				
Particle diameter, m: 50				
Reactor Pressure, psig (bar): 174 (12)				
Weight Fraction Catalyst in Slurry: 0.20				
Specific Heat Transfer Area, cm^2/cm^3: 0.30				
Inlet Gas Velocity, cm/sec: 9				
Temperature, C: 260.0				
Preexponential Factor (see wt% in slurry): 3.45×10^7				
Activation Energy, kJ/mol: 94l7				
Inlet Ratio, mol CO/mol H_2: 1.98				
Usage Ratio, mol CO/mol H_2: 1.98				

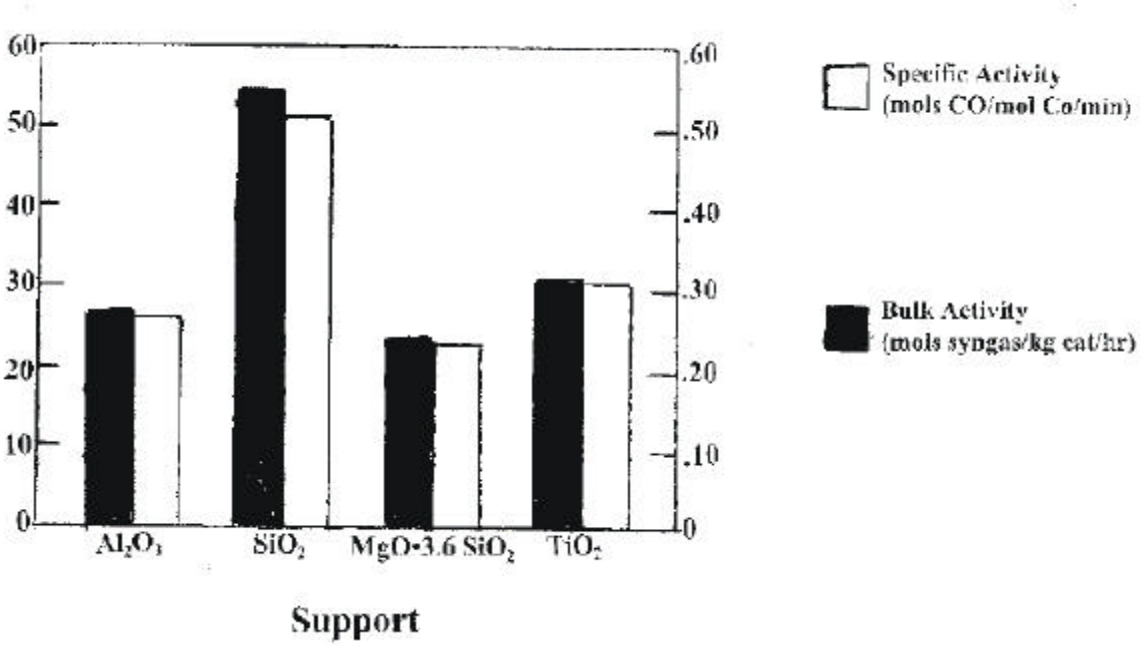

Figure IX.1. Activity of $CO_2(CO)_8$-based catalysts, fixed bed reactor (240°C, CO/H_2 = 1.0, GHSV = 1000 hr^{-1}, 300 psig).

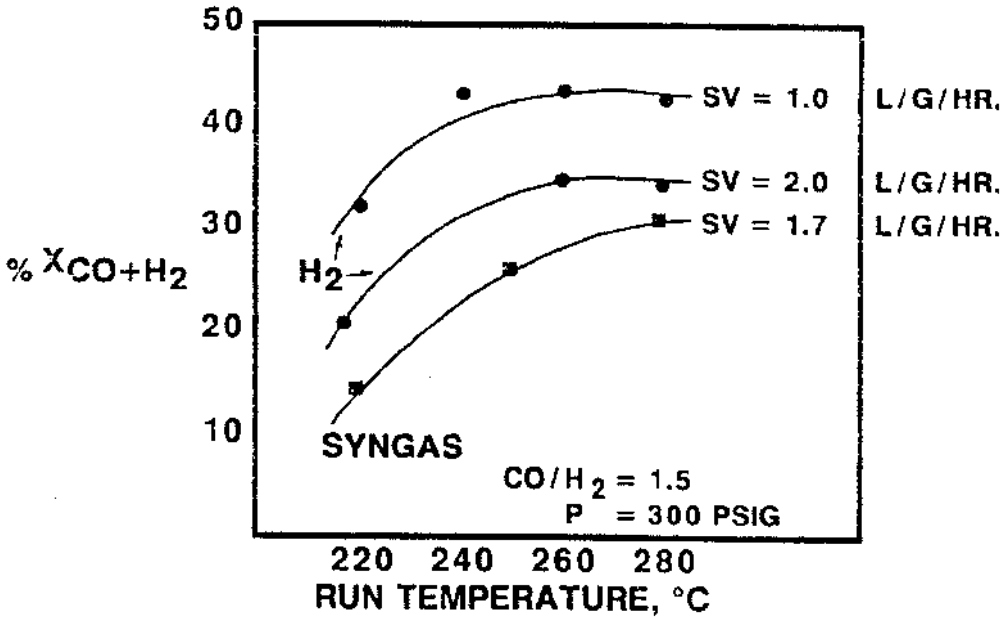

Figure IX.2a. Effect of syngas versus hydrogen activation on conversion.

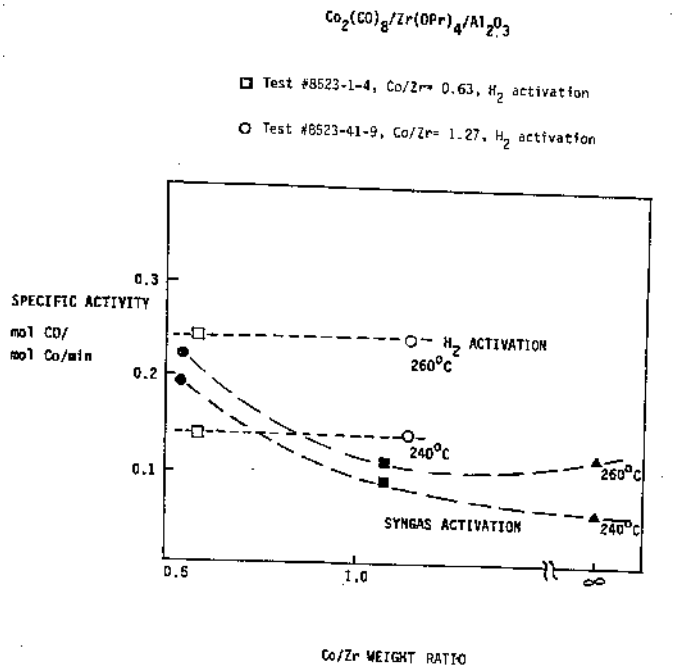

Figure IX. 2b. CO/Zr ratio effect on activity.

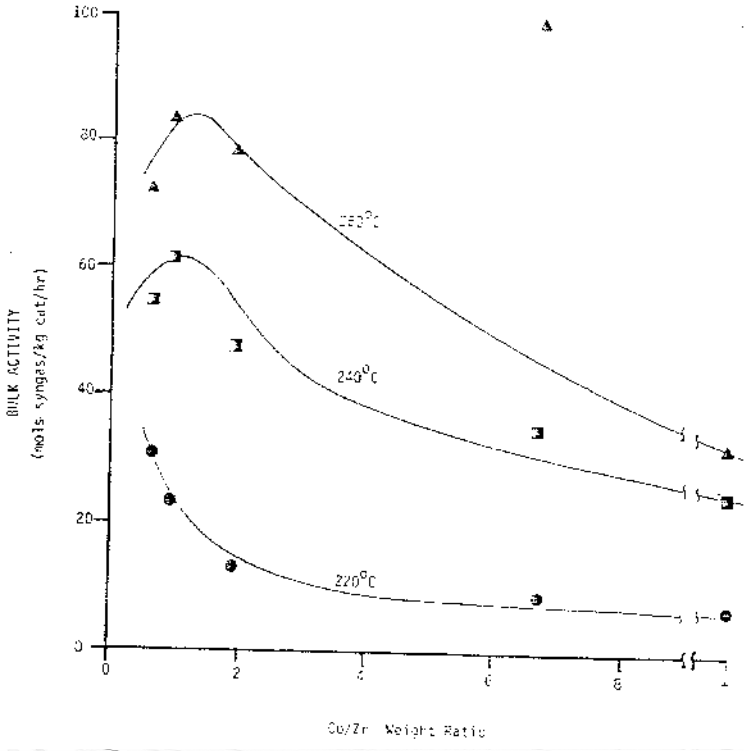

Figure IX.3. Effect of Co/Zr ratio on bulk activity (gas phase, CO/H_2 = 1, SV = 1000 hr^{-1}, 300 psig).

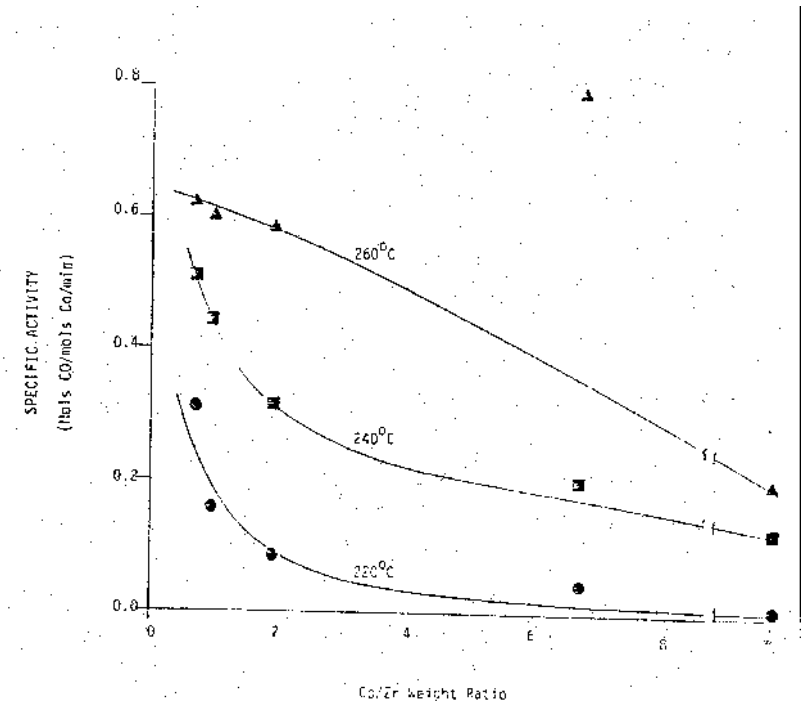

Figure IX.4. Effect of Co/Zr ratio on specific activity (gas phase, CO/H_2 = 1, SV = 1000 hr^{-1}, 300 psig).

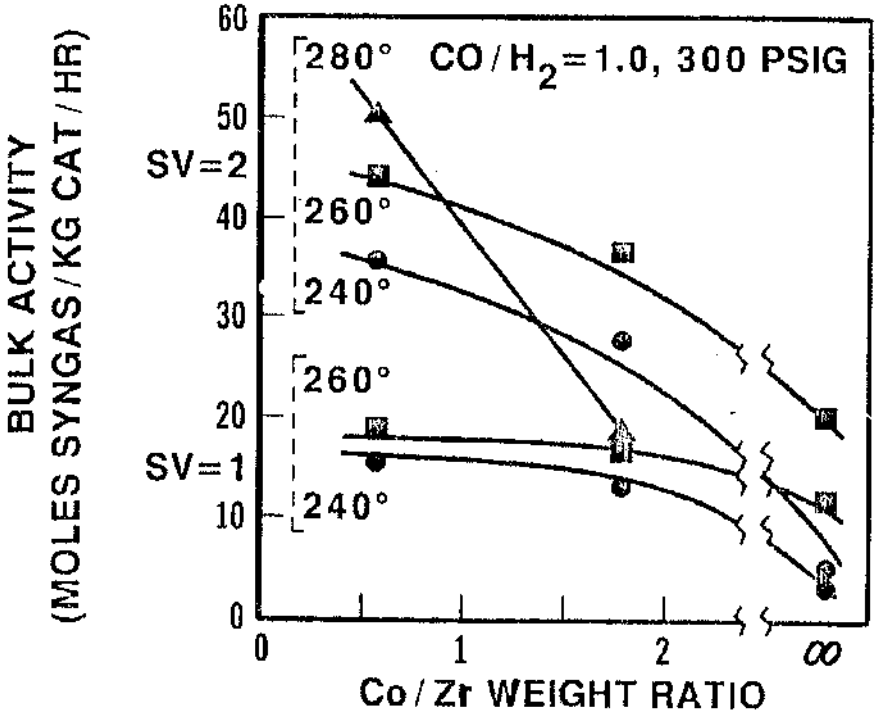

Figure IX.5. Effect of Co/Zr weight ratio on slurry-phase activity of Co/Zr/silica catalysts.

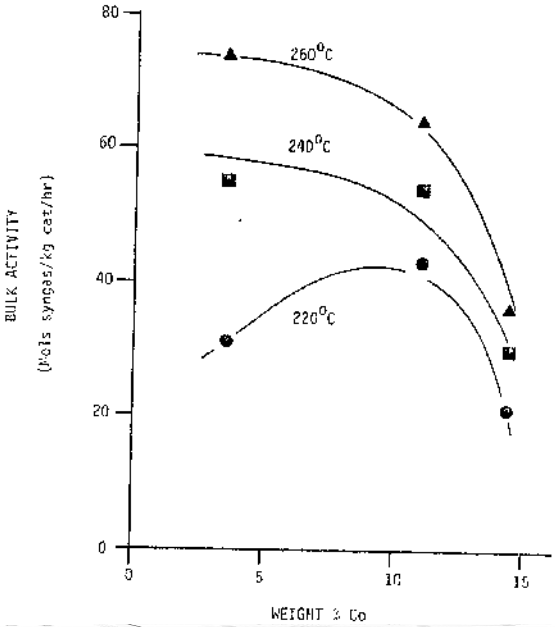

Figure IX.6. Effect of cobalt loading on bulk activity of $Co/Zr/SiO_2$ Catalyst (fixed bed reactor , $CO/H_2 = 1$, 1000 hr^{-1}, 300 psig).

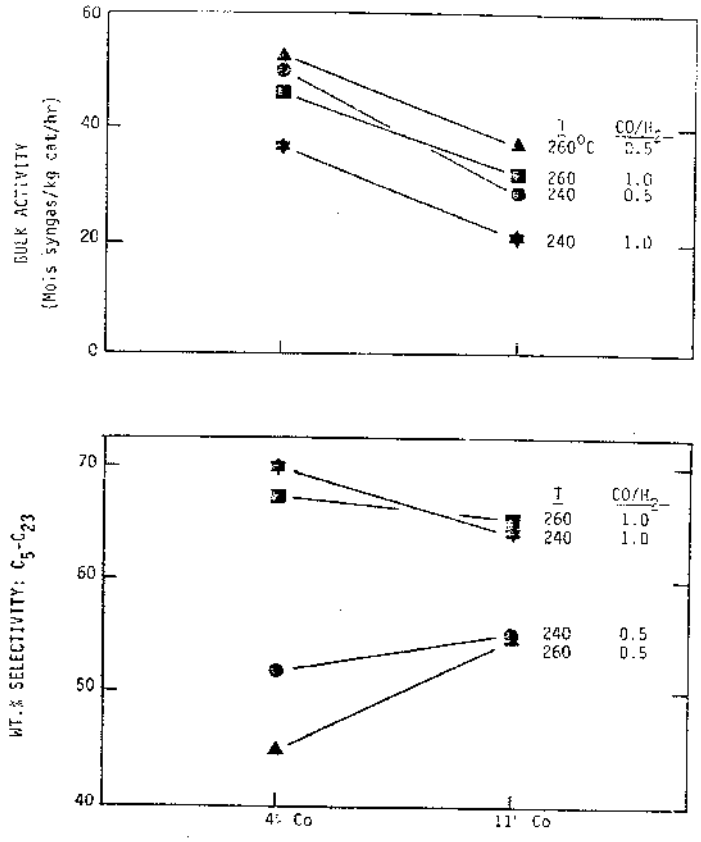

Figure IX.7. Effect of Co loading on $Co/Zr/SiO_2$ performance.

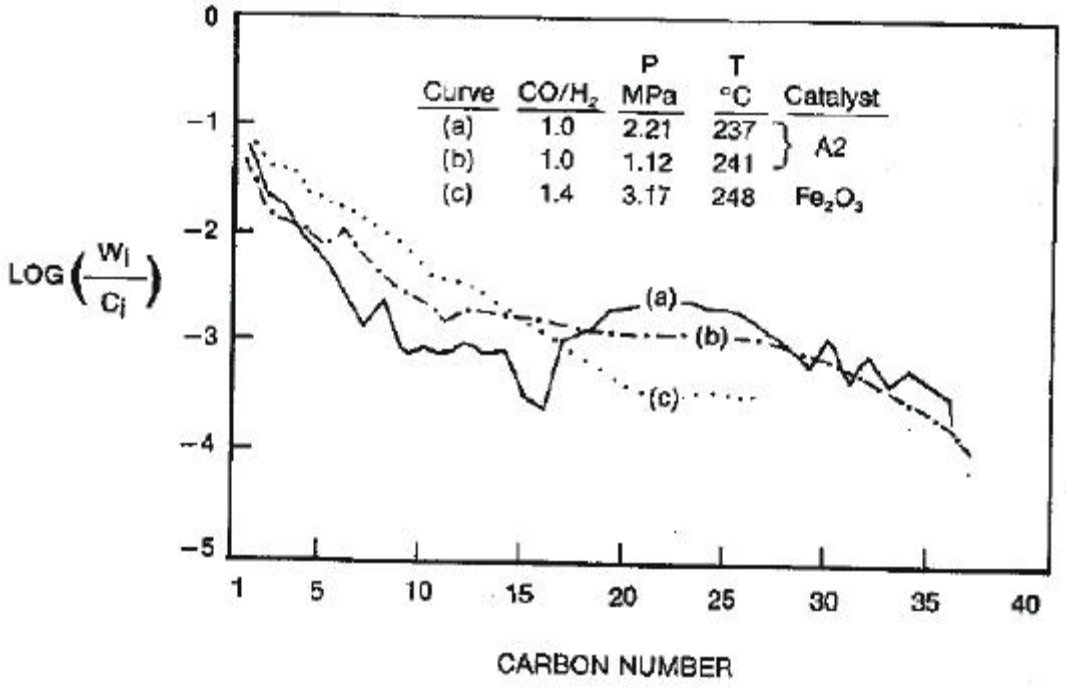

Figure IX.8. Hydrocarbon Schulz-Flory distribution of slurry catalyst A2.

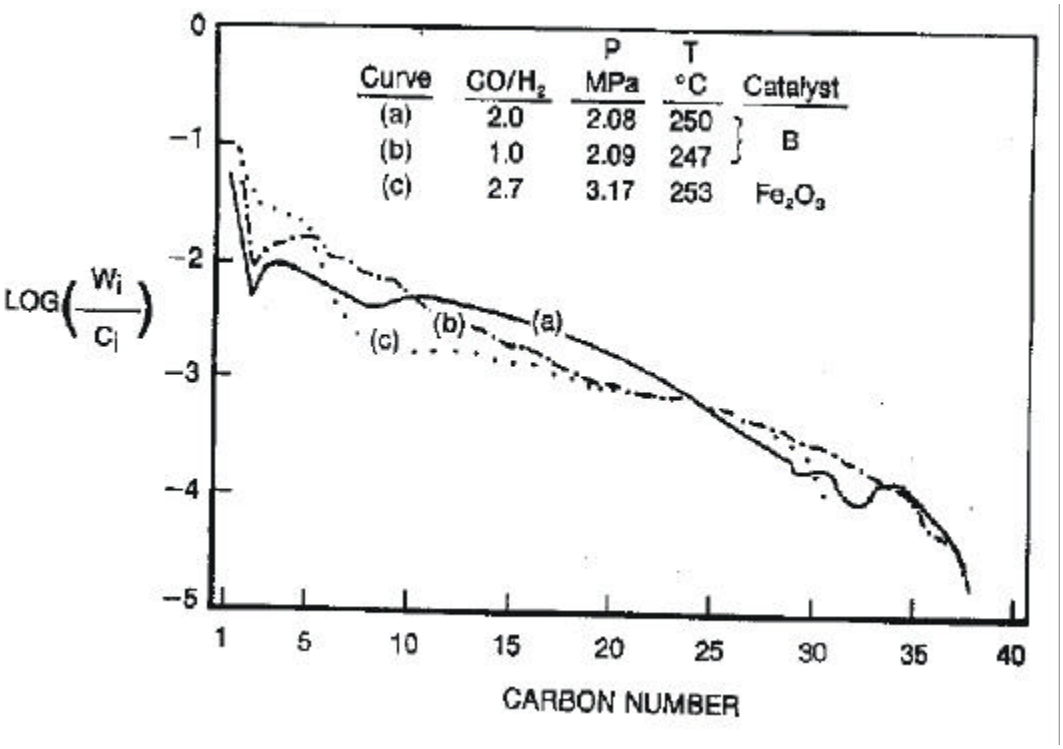

Figure IX.9. Hydrocarbon Schulz-Flory distribution of slurry catalyst B.

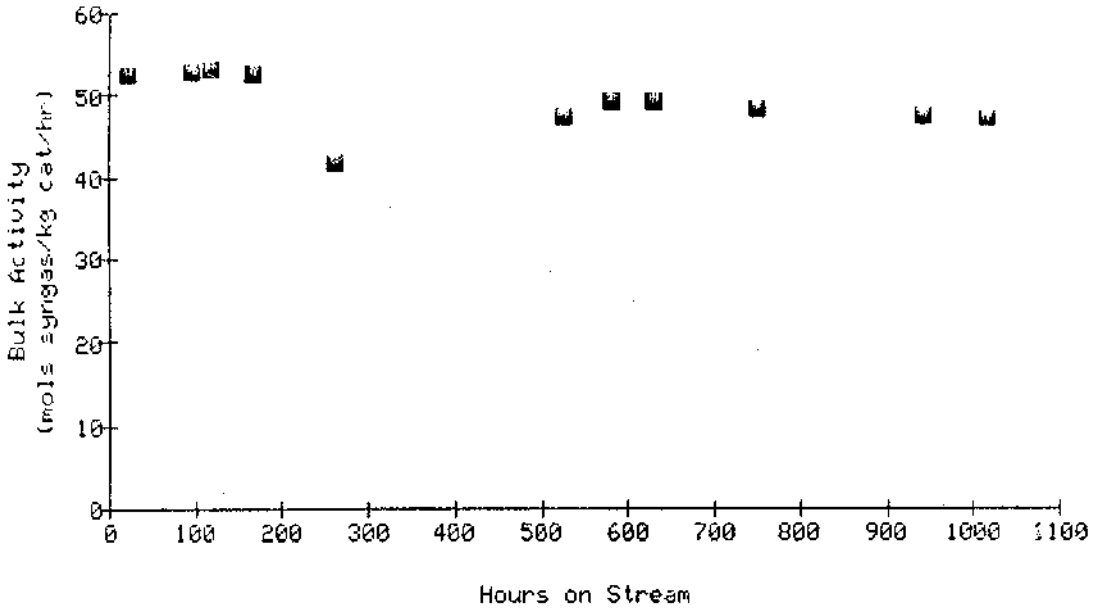

Figure IX.10. Bulk activity maintenance - extended slurry test 8862-1-31 $Co/Zr/SiO_2$, 240°C, CO/H_2 = 0.5, 1.8 L/g/hr, 300 psig.

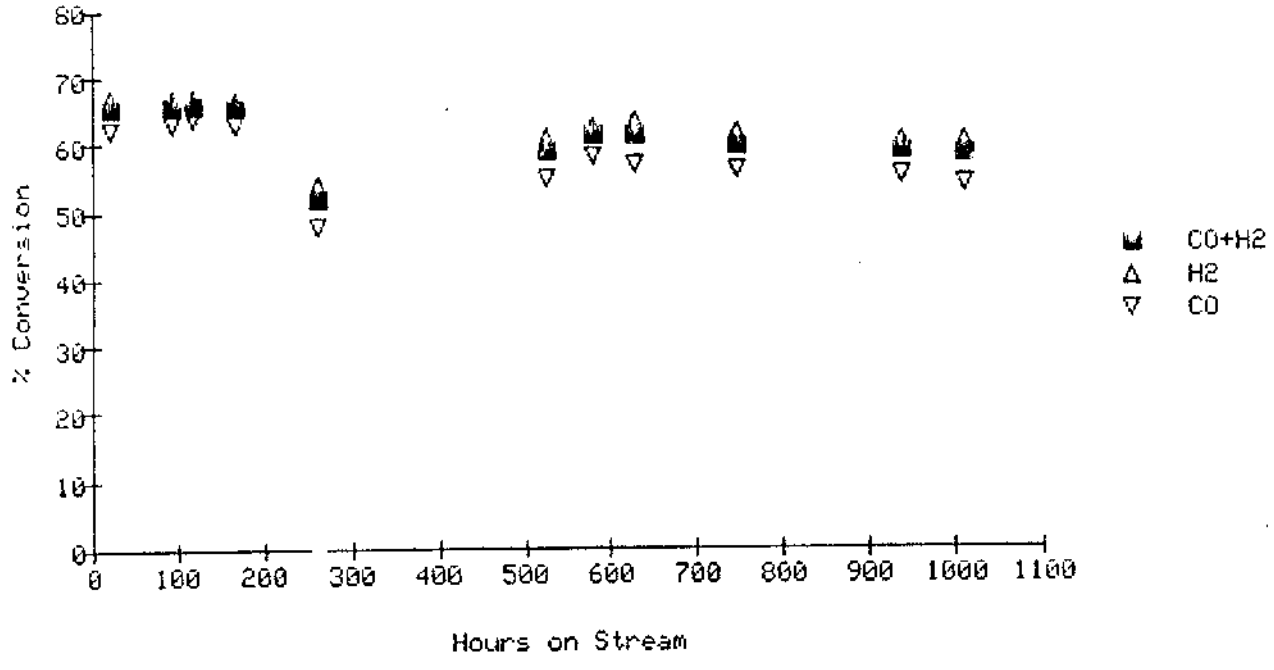

Figure IX.11. Conversion maintenance - extended slurry test 8862-1-31 $Co/Zr/SiO_2$, 240°C, CO/H_2 = 0.5, 1.8 L/g/hr, 300 psig.

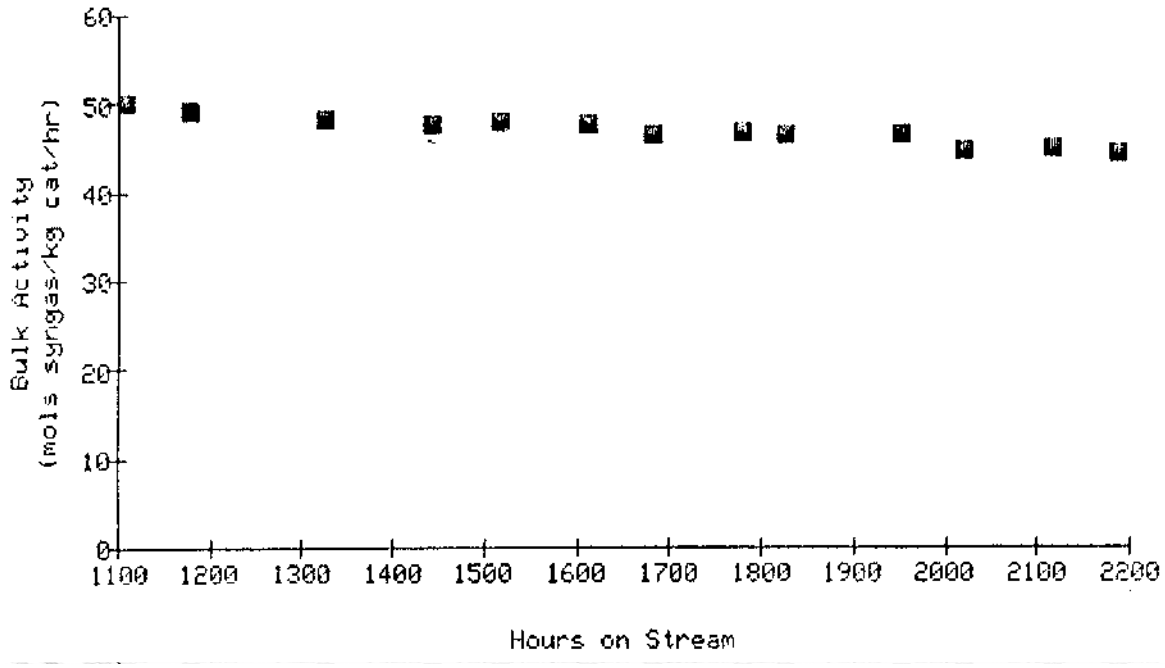

Figure IX.12. Bulk activity maintenance - extended slurry test 8862-1-31 ($Co/Zr/SiO_2$, 260°C, CO/H_2 = 1.0, 2.0 NL/g/hr, 300 psig).

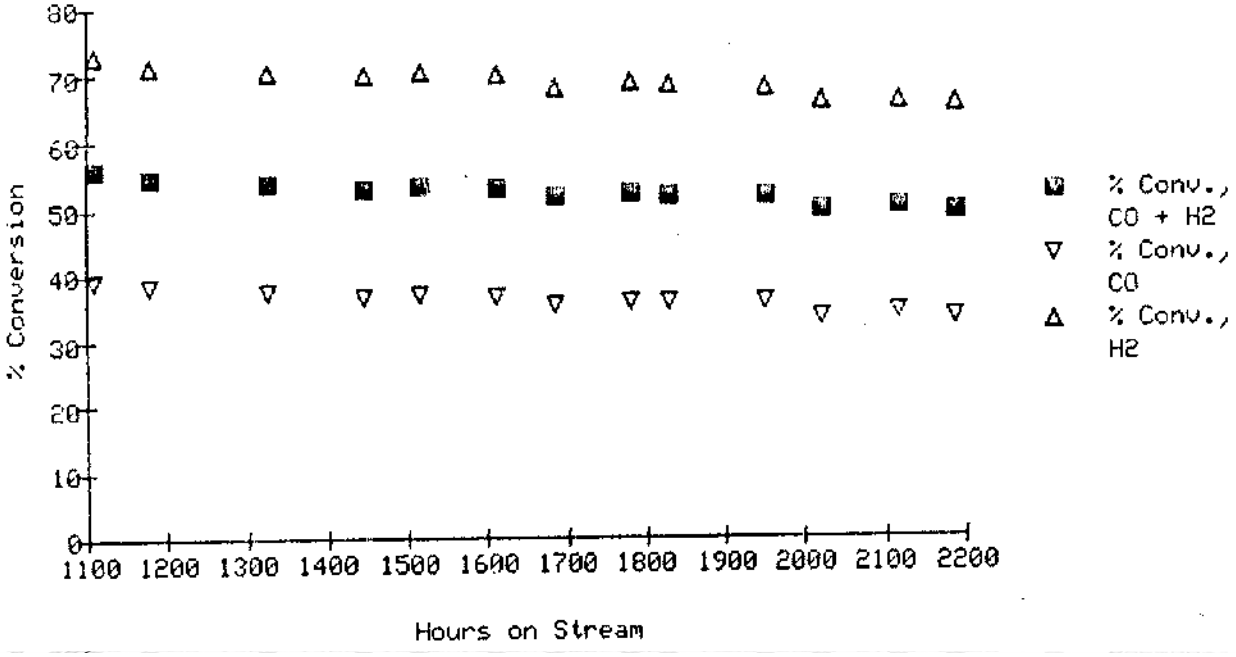

Figure IX.13. Conversion maintenance - extended slurry test 8862-1-31 ($Co/Zr/SiO_2$, 260°C, CO/H_2 = 1.0, 2.0 NL/g/hr, 300 psig).

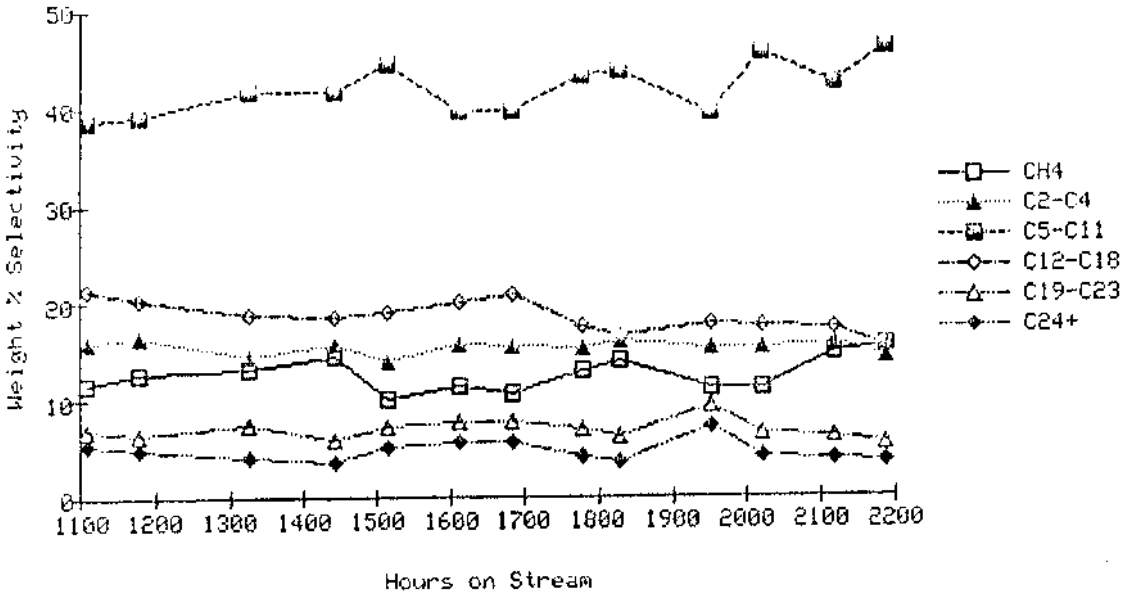

Figure IX.14. Hydrocarbon selectivity — extended slurry test 8862-1-31 ($Co/Zr/SiO_2$, 260°C, CO/H_2 = 1.0, 2.0 NL/g/hr, 300 psig).

Figure IX.15. Kinetic data analysis program (? = 0.758-0.555•(T_k-373) (ref. 12);

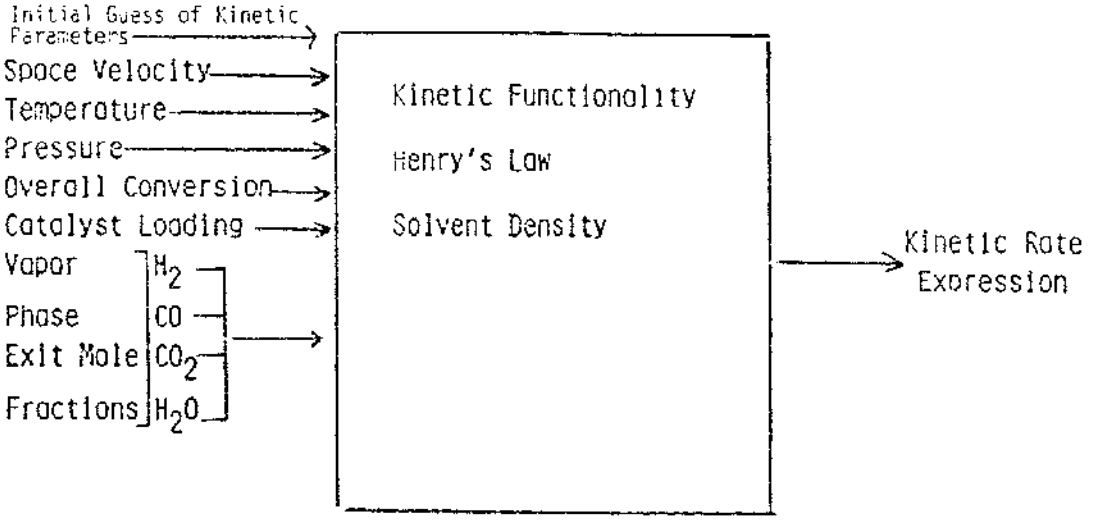

He_{H_2} = 34.162 •exp (739.485/T_k)•14.23 psia/mol/kg oil (ref. 11); He_{CO} = 44.583/T_k)•exp (433.391/T_k)•14.23; He_{CO_2} = 119.925•exp (-438.926/T_k)•14.23; He_{H_2O} = 275.113 • exp (-1122.92/T_k) • 14.23.

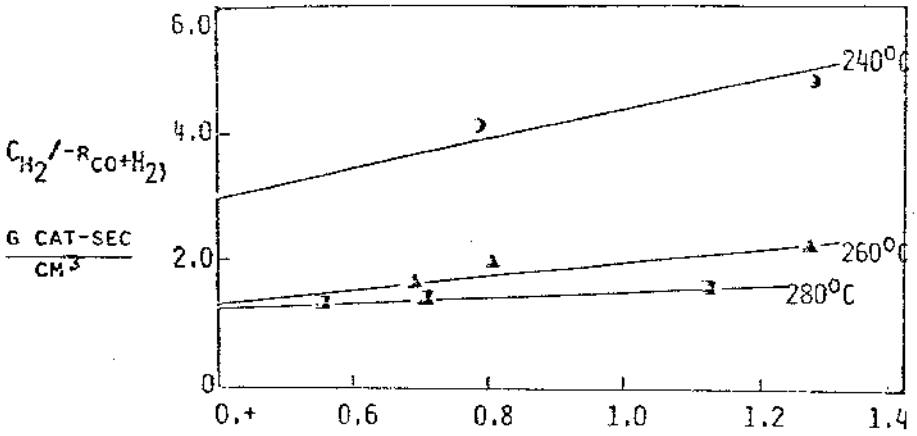

	K, CM³/G CAT.SEC.	K
240	0.328	0.466
260	0.709	0.439
280	0.775	0.302

Figure IX.16. Fitting $Co_2(CO)_8/Zr(OP_R)_4/SiO_2$ data.

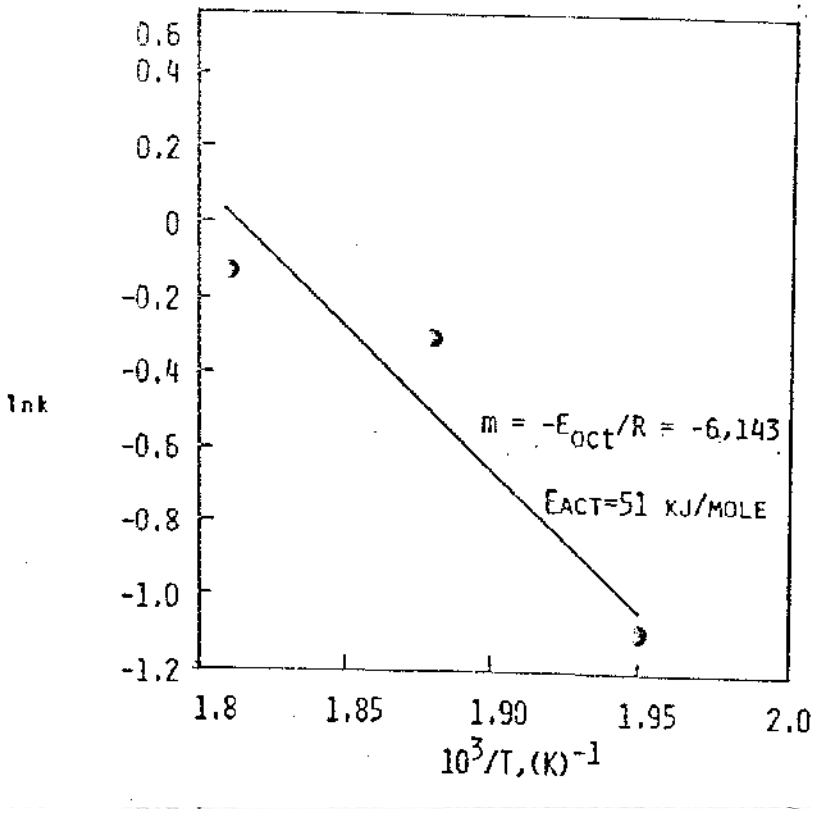

Figure IX.17. $Co_2(CO)_8/Zr(OP_R)_4/SiO_2$ activation energy.

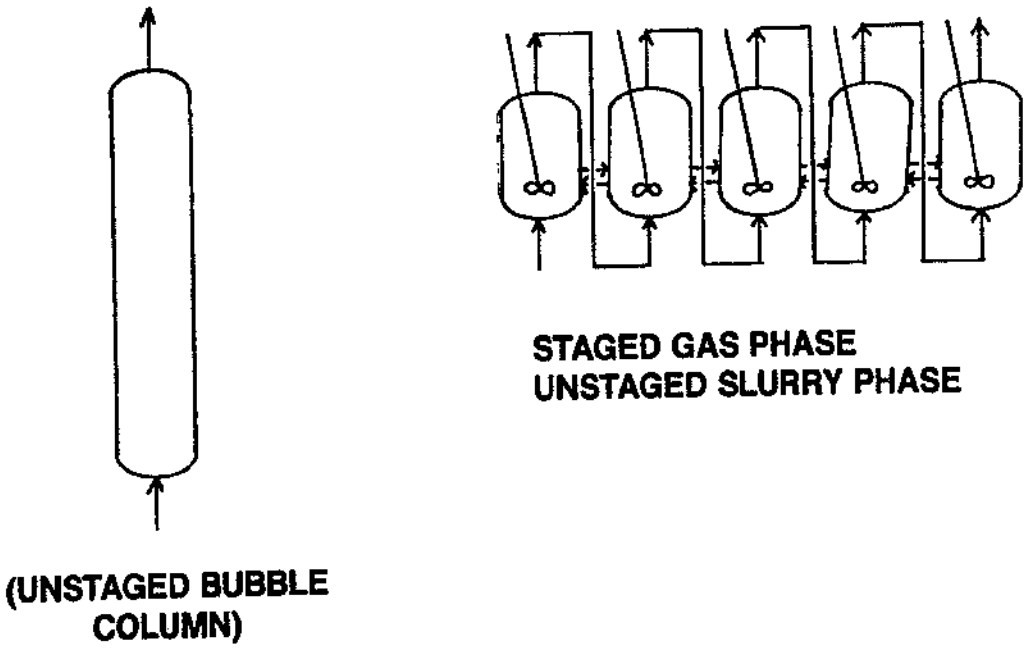

Figure IX.18. Staged reaction systems.

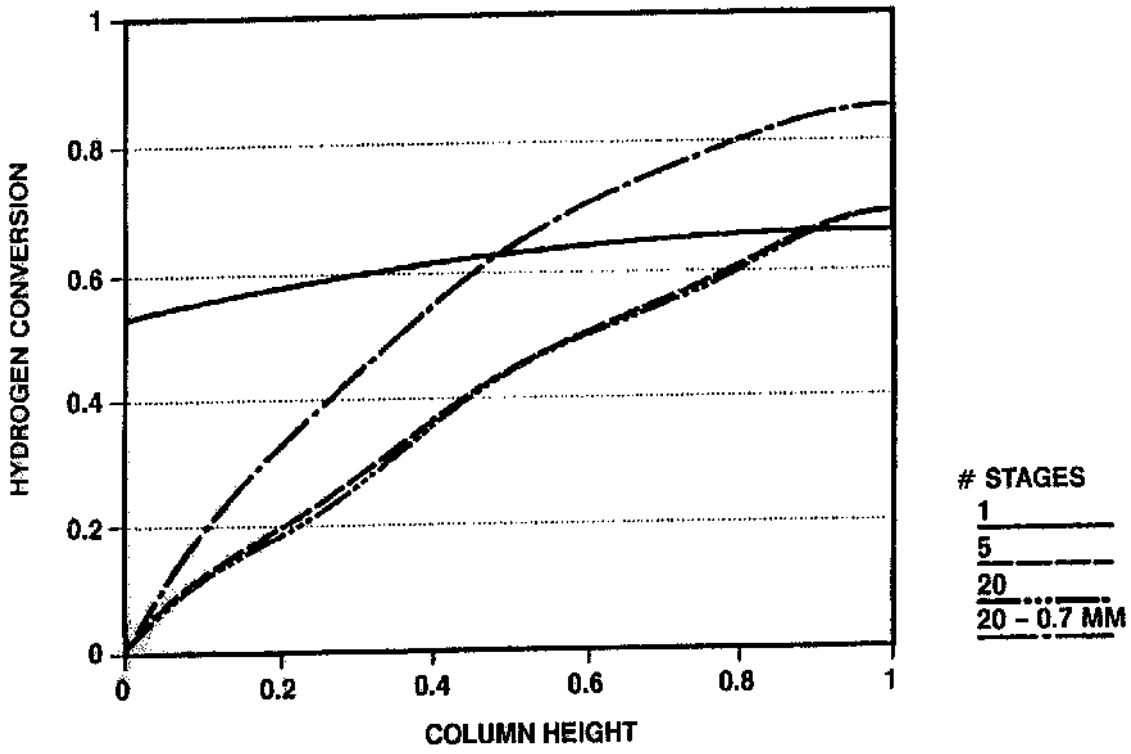

Figure IX.19. Hydrogen conversion vs. column height.

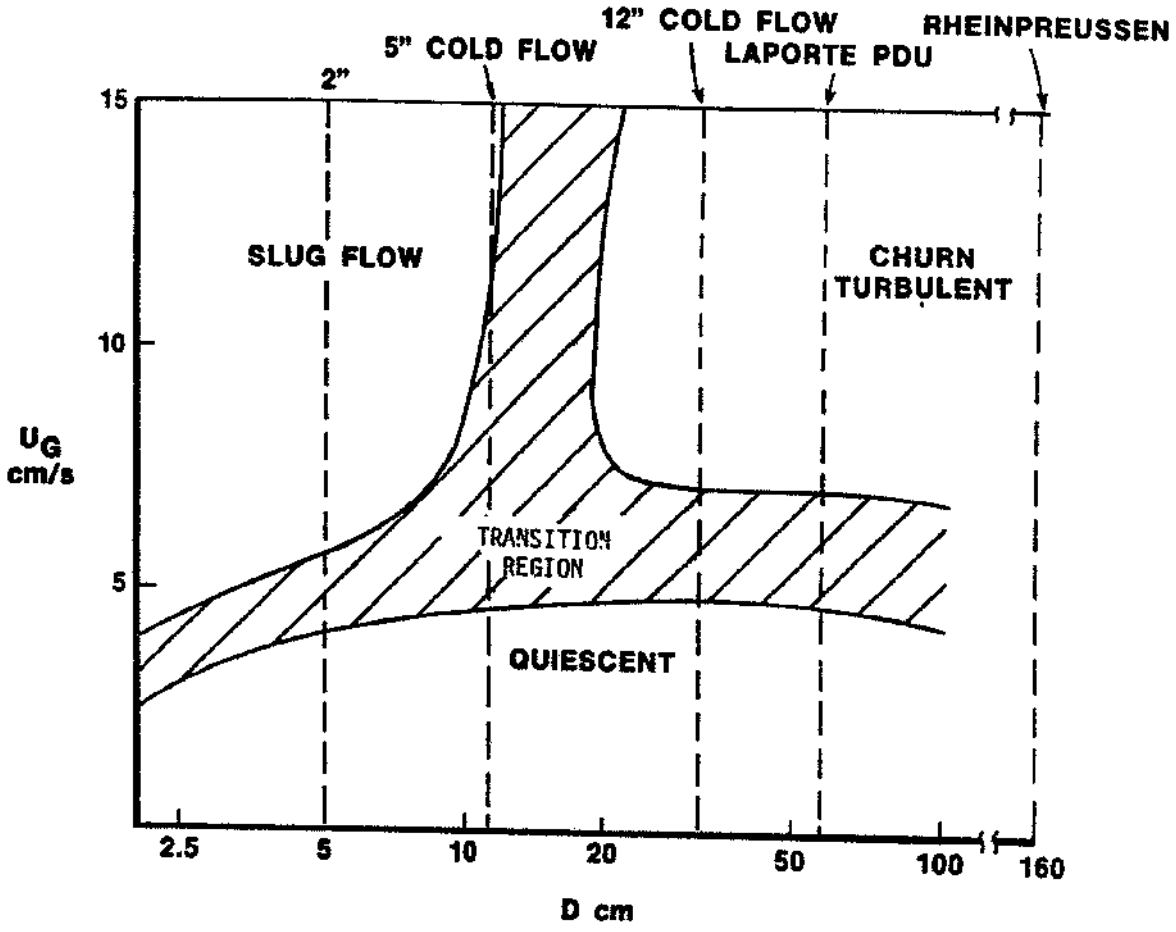

Figure IX.20. Bubble column flow regimes.